JOURNAL OF AIRCRAFT
Vol. 41, No. 5, September–October 2004

Transition on a High-Lift Swept Wing in the European Project EUROLIFT

Jean Perraud* and Alain Séraudie†
Office National d'Etudes et de Recherches Aérospatiales (ONERA), BP 4025, 31055 Toulouse Cedex, France
and
Frédéric Moens‡
Office National d'Etudes et de Recherches Aérospatiales (ONERA), BP 72, 92322 Châtillon Cedex, France

Performance of transport aircraft in high-lift conditions is directly related to the maximum lift. However, most of the high-lift tests are carried out at subscale conditions, and performance is then derived by extrapolation to flight Reynolds number. So-called adverse Reynolds number effects (sudden decrease of maximum lift with increasing Reynolds number) often occur when extrapolations from the wind-tunnel and flight-tests results are compared. Most of these effects are due to changes in the transition process. Improvement of the knowledge of the transition process for three-dimensional high-lift configurations is, thus, necessary. Therefore, specific experimental and numerical tasks were decided on within the European research project EUROLIFT, dedicated to high-lift aerodynamics. Within this program, a generic high-lift swept wing was first tested by the use of wall hot films and infrared thermography in the ONERA F1 pressurized wind tunnel to study Reynolds number effects on transition. This test campaign provided a detailed database for the transition prediction tools developers and for the assessment of numerical methods. Based on accurate pressure distributions obtained from three-dimensional Navier–Stokes computations, a theoretical and numerical study of transition was conducted based on both exact and simplified stability approaches. Results contributed to a better understanding of transition phenomena in high-lift conditions, as well as to extension of the validity of methods and rules used to predict attachment line contamination, relaminarization, and stability-based transition.

Nomenclature

$C_{p,\text{norm}}$	=	normalized pressure coefficient, theoretically independent of the sweep angle, $C_p/(\cos\varphi)^2$
C_0	=	reference chord length of the model at 0-deg sweep, without slat and with retracted flap
F	=	nondimensionalized frequency of instability, $2\pi f\nu/U_e^2$
H_I	=	incompressible shape factor, ratio of the displacement thickness δ_1 to the momentum thickness θ, δ_1/θ
K	=	acceleration parameter, $(\nu/U_e^2)(\partial U_e/\partial x)$
P_i	=	parameter of the crossflow simplified model, $y_i(\partial U/\partial y)_{y_i}$
Re	=	Reynolds number based on the projected reference wing chord $C_0/\cos(\varphi)$
R_l	=	Reynolds number based on length l
$\bar{R}$	=	attachment line contamination Reynolds number, $W_e/\sqrt{[\nu(\partial U_e/\partial X)_{X_a}]}$
U_i	=	boundary-layer velocity at the height of the inflection point
W_e	=	spanwise velocity component, in z direction
y_i	=	height of the inflection point on the boundary-layer profile
y^+	=	wall scale, yU_τ/ν
α	=	model incidence
α_F	=	flap deflection, 20 or 40 deg
ν	=	kinematic viscosity
σ	=	growth rate of the instabilities
υ, β	=	wave numbers of instability waves
φ	=	model sweep angle
ω	=	nondimensionalized pulsation, FR_{δ_1}

Presented as Paper 2003-3796 at the 21st Applied Aerodynamics Conference, Orlando, FL, 23 June 2003; received 1 August 2003; revision received 14 October 2003; accepted for publication 18 October 2003.

*Research Engineer, Aerodynamics and Energetics Model Department; Jean.Perraud@onecert.fr. Member AIAA.
†Research Engineer, Aerodynamics and Energetics Model Department.
‡Research Engineer, Applied Aerodynamics Department.

Introduction

THE maximum lift of multi-element high-lift swept wing configurations has been thus far determined in wind-tunnel experiments; three-dimensional codes, in particular, do not yet guarantee sufficient accuracy and turn-around time. However, most of these high-lift tests are carried out at subscale conditions, and aircraft characteristics are derived by extrapolation to flight Reynolds number. Such extrapolation requires a good understanding of the transition process and its changes with Reynolds number.

Moreover, a given section of a wing in high-lift configuration is generally composed of several airfoils of different geometry: a leading-edge slat, a main wing, and the flap system. Because of different profiles and local conditions, transition processes of different natures can be observed on each element, which makes the evaluation of a change in Reynolds number very difficult. Therefore, within the European research project EUROLIFT,[1,2] which deals with high-lift aerodynamics, specific experimental and numerical tasks were decided on for the study of transition on a generic high-lift swept-wing configuration, called Aile à Flèche Variable (AFV). A wind-tunnel test campaign dedicated to this topic has been carried out, with the objective of providing a detailed database for the transition prediction tool developers and for the assessment of numerical methods. Experiments[3] took place in the ONERA F1 pressurized wind tunnel at le Fauga–Mauzac Center, over a wide range of Reynolds numbers. In a separate project task, three-dimensional Reynolds-averaged Navier–Stokes (RANS) computations were undertaken to assess the prediction of maximum lift and of stall and to generate surface pressure distributions. These were the input to a third task, dedicated to transition prediction.

At large angles of incidence, transition from laminar to turbulent flow may occur in several distinct ways. At low Reynolds numbers, short bubble transition is often observed. Then, with increasing

Reynolds number, transition moves upstream of separation and is controlled by boundary-layer instabilities. At even larger Reynolds numbers, attachment line contamination will occur, sometimes followed by relaminarization. Each of these phenomena must be correctly predicted.

An increase of the capacity of computational tools requires validation of models that were developed during these past few years for aircraft wings in cruise conditions (high Reynolds numbers). For transition controlled by boundary-layer instabilities, methods are based on the linear stability theory, either in its local [Orr–Sommerfeld, (OS)] or nonlocal [parabolized stability equations (PSE)] formulation. Turn-around time reduction in transition prediction is also a major goal because stability computations are difficult and time consuming. Introduction of simplified methods is a promising development because they require little analysis time compared to analyses that use methods based on resolution of the OS or PSE. ONERA has developed such simplified methods[4,5] in the course of past European research programs. In EUROLIFT, they were distributed to the project partners involved in transition prediction for implementation in various codes and for validation.

Experiments

EUROLIFT partners to the AFV experimental task were Airbus-D (Germany), Swedish Defense Research Agency (FOI) (Sweden), Alenia and Centro Italiano Ricerche Aerospaziali (CIRA) (Italy), Airbus-España (CASA) (Spain), and ONERA and Dassault Aviation (France), with ONERA as task leader. These tests were, in a sense, preliminary to more realistic experiments in the European Transonic Wind Tunnel at large Reynolds numbers, in which another model was used and that took place within other EUROLIFT tasks.[6] The greater simplicity of the AFV configuration was selected to allow in-depth investigation of transition phenomena and their prediction.

Model Description and Test Setup

Experiments took place in the F1 ONERA low-speed pressurized wind tunnel located at the ONERA le Fauga–Mauzac Center at the end of the year 2000. Pressurization allows a modification of the Reynolds number while the Mach number is kept constant.

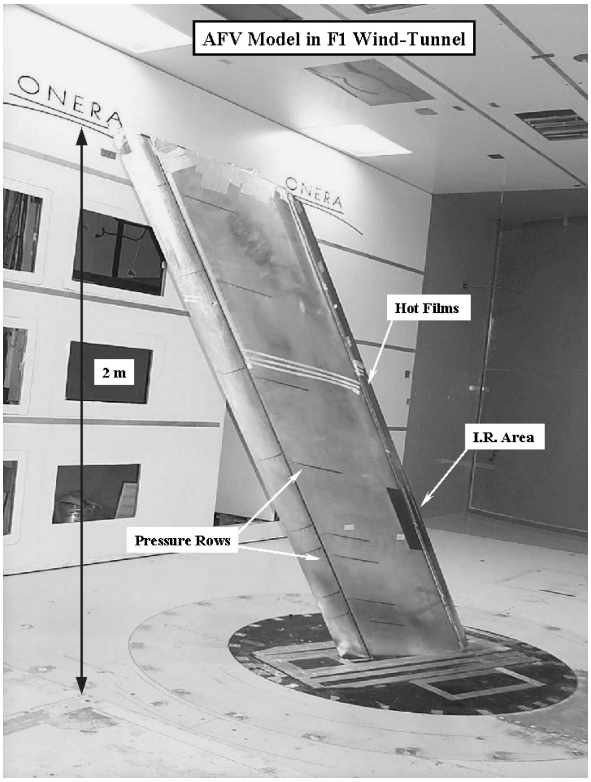

Fig. 1 AFV model in F1 ONERA wind tunnel.

Table 1 Reference geometrical values according to sweep angle

Sweep, deg	One-half span, m	C_{ref}, m	S_{ref}, m^2
40	2.000	0.653	1.305
30	2.282	0.577	1.329

Fig. 2 Hot films locations on the AFV model (elements not to same scale).

The model used (AFV wing, Fig. 1) is a rectangular untwisted wing, based on a three-element airfoil configuration. Geometrical definitions are given for streamwise cuts at 0-deg sweep. In that case, the basic geometry is the RA16SC1 airfoil, equipped with a leading-edge slat. The reference chord in that case is $C_0 = 0.5$ m, corresponding to the chord with flap retracted and without slat. Slat deflection is fixed (30 deg), and there are two different possible flap settings (α_F) of 20 and 40 deg. Sweep angle can vary from 0 to 50 deg, with discrete values of 10 deg. Changing the sweep angle modifies the reference geometrical values according to Table 1.

The model is mounted right above the wind tunnel floor, with no separation; hence, it is subjected to possible contamination by the floor boundary layer. It is equipped with 8 rows of 93 pressure taps each, distributed over the 3 elements: 20 taps on the slat, 47 on the main wing, and 26 on the flap. There is, therefore, a total of 744 pressure taps on the model, connected to electronic pressure scanners from "Pressure Systems Inc. (PSI)," which allows fast recording to be carried out in parallel to the balance measurements. Pressure rows, tracks fairing (for slat and flap), and the wing tip are parallel to the floor for a 40-deg sweep.

In the EUROLIFT test campaign, the AFV model was tested at two sweep angles, $\varphi = 30$ and 40 deg, and Reynolds numbers from 3×10^6 to 10×10^6, at Mach 0.2. Two sets of data have been considered for force and pressure measurements:

For the continuous polar data, the angle of attack increases from -5 deg up to $CL_{\max}$ and beyond, at a continuous speed of 0.2 deg/s. There is one C_P record per second during this phase.

The stabilized points data are for the detailed transition measurements. About 10 C_P records are done to check the flow stability. There are about seven stable points recorded per aerodynamic condition.

It was verified that these two types of acquisition give the same results.

A wall balance measured forces and moments during the tests, and accelerometers measured the vibration level. Transition detection was performed with infrared thermography and wall hot films distributed along a chordwise section of the three elements (Fig. 2). The slat element length is 0.12 m, and the flap is 0.145 m.

A region of the slat upper side and of the wing leading edge was covered with a thin layer of specific black paint, visible in Fig. 1, that ensured a large enough emissivity coefficient. The infrared camera was installed just behind the test-section right vertical wall.

There were 24 Dantec hot films distributed on the 3 parts of the model (Fig. 2), on the slat (9), the wing (9), and the flap (6). They were glued directly on the metallic wing, and electrical connections were realized with thin copper strips.

Summary of Experimental Results

Major results concerning transition and pressure measurements are presented here. Two aspects of transition are discussed in this section; other results will later be compared to numerical predictions. Experimental result were also presented and discussed in a previous paper.[3] In what follows, the Reynolds numbers are based on the projected reference wing chord C_{ref}, not on the element dimension.

Experimental pressure distributions were used to validate the use of infinite swept-wing theory on this configuration. The infinite sweep law $[C_p/(\cos\varphi)^2 = C_{p,\text{norm}}$, independent of sweep angle] generally proved applicable (Fig. 3), with the exception of the accelerated part of the upper slat surface at large incidence. Transition is, in that case, caused by early separation, not by slow instability growth. Hence, the infinite sweep law may be used for the theoretical work on transition prediction: Pressure distribution for $\varphi = 30$ deg can be built from a $\varphi = 40$ deg solution.

In addition, for a given sweep, there was no major Reynolds number effect observed on the measured pressure distribution, on the different elements at a given section, either for low or high angle of attack, as shown in the case of the slat element (Fig. 4).

The computational fluid dynamics (CFD) computations needed to provide an accurate estimation the pressure distribution on the different elements for transition prediction study could, therefore, be carried out by the use of only $\varphi = 40$ deg at a single Reynolds number of 7.5×10^6.

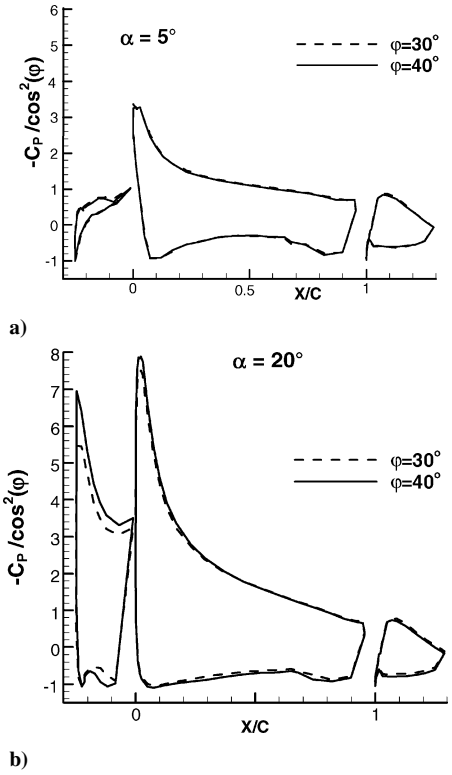

Fig. 3 Normalized measured pressure distributions at 30- and 40-deg sweep, at a) 5-deg and b) 20-deg incidence ($Re = 7.5 \times 10^6$ and $\alpha_F = 20$ deg).

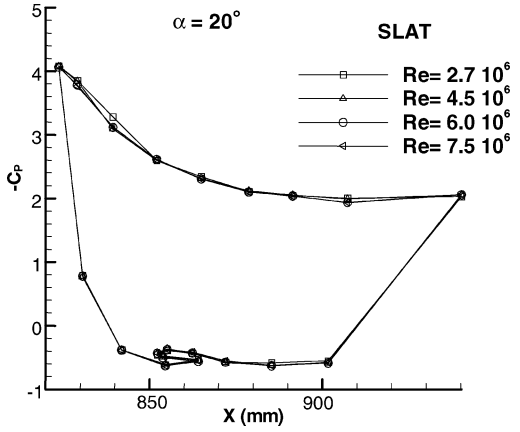

Fig. 4 Measured pressure distributions at various Reynolds number values on the slat element ($\alpha = 20$ deg, $\varphi = 40$ deg, and $\alpha_F = 20$ deg).

Two measurement techniques were used to detect transition, surface hot films and infrared visualization. The first is sensitive to skin friction and the second to thermal exchange, two closely related phenomena. Infrared thermography was used by the imposition of a small thermal imbalance. The flow temperature is first allowed to increase from 8 to 10°C above its initial value, then temperature regulation is reimposed, causing a rapid drop of flow temperature, faster than that of the model wall. When flow temperature is about 2°C above its steady value, infrared images are recorded with a hot wall condition; hence, laminar regions appear white and turbulent ones are darker.

The transition location was determined by measurement of the extent of the clear laminar region close to the leading edge. This location generally corresponds to the middle of the transition region. Typical infrared images are shown in Fig. 5 for $Re = 3 \times 10^6$. These images show the slat upper surface and a small part of the main wing upper surface. At 5-deg incidence, white laminar and gray turbulent regions are visible, but the frontier between the two is difficult to define on the reproduced pictures. At 20-deg incidence, the change is brutal and a line is visible between white and gray. These different evolutions will later be related to crossflow and short bubble transition.

Hot-film signals are also useful in the location of transition. Fluctuation levels usually evolve from a very low level in the laminar region to a peak in the transition region, then fall to an intermediate level, larger than the laminar one, in the turbulent region.

The first rise generally corresponds to the beginning of transition. A comparison of infrared to hot-films results on the slat

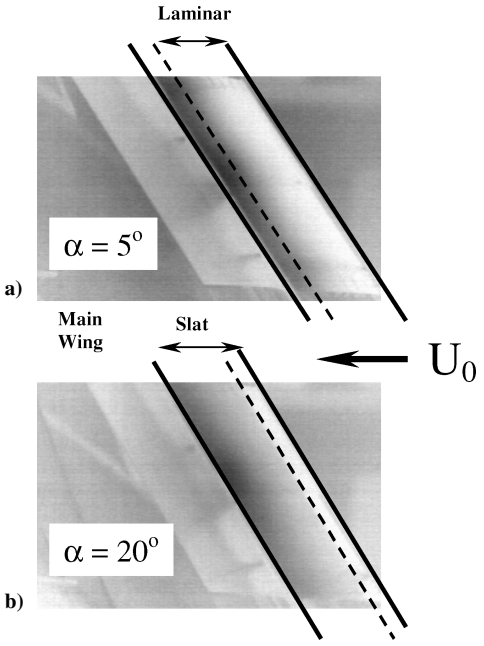

Fig. 5 Typical infrared images: a) $\alpha = 5$ deg and b) $\alpha = 20$ deg ($\varphi = 40$ deg, $Re = 3 \times 10^6$, and $\alpha_F = 40$ deg).

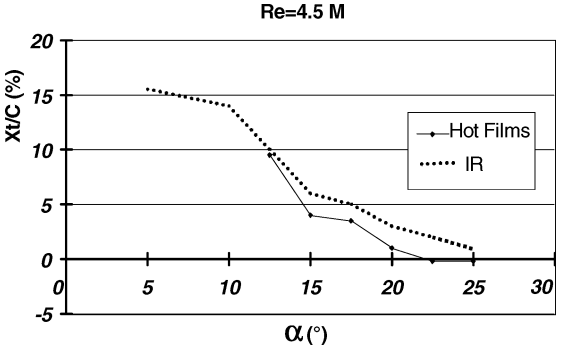

Fig. 6 Transition location on the slat upper surface from infrared and hot films at $Re = 4.5 \times 10^6$ and $\alpha_F = 40$-deg.

upper surface (Fig. 6) shows a small difference at $\alpha = 12.5$ deg and an increasing distance between the two measurements at larger incidences. Comparison is not possible at low incidence because the last hot film is located at $X/C = 12.7\%$. At large incidences, hot films still indicate the beginning of transition, but infrared show instead the location of reattachment in the case where transition occurs in a separation bubble. In such a case, the reattachment line is clearly visible on Fig. 5b.

Attachment Line Contamination

Because the model is fixed to the wind-tunnel floor and is not equipped with a Gaster bump, attachment line contamination is a concern. This contamination is due to the transport of floor (or fuselage) turbulence along the attachment line of the wing. Increased sweep and large curvature radius in the leading-edge region promote this transport. When this occurs, the whole wing surface becomes turbulent, with no laminar region. Pretest RANS computations in the reference case ($\varphi = 40$ deg and $\alpha_F = 20$ deg) provided useful information to select a second sweep angle of 30 deg to avoid main wing systematic contamination.

Attachment line contamination is characterized by the parameter $\bar{R} = W_e/\sqrt{[\nu(\partial U_e/\partial X)_{X_a}]}$, with X_a referring to the attachment line. It can be shown to vary as the square root of the Reynolds number, or of the nose radius, and increases with sweep. Critical value[7,8] of the $\bar{R}$ parameter is usually taken as 250 ± 20. Calculation of $\bar{R}$ first requires the knowledge of the effective sweep angle from which $W_e = Q_e \sin(\varphi_{\text{eff}})$ is obtained. In the present case, an iterative method is used to look for a linear evolution with distance to the attachment line of the normal to leading-edge velocity $Q_e \cos(\varphi_{\text{eff}})$. The location of this attachment line is determined in the process. $\bar{R}$ was determined from RANS pressure field data, before and after the wind-tunnel tests.

Figure 7 shows typical evolutions obtained from computed pressure distributions on the slat and the main wing of the AFV model, which show that the main wing should always be contaminated at 40-deg sweep and the slat at large Reynolds numbers. The attachment line Reynolds number for the flap remained below 250 over the entire range of flow conditions considered in the experiment, and, hence, attachment line transition was not considered an issue for this element. Predictions presented here were verified in the experiment.

Rapid evolution of $\bar{R}$ in the first 0.5 m above the floor is due to variations of the effective sweep angle. An infinite swept-wing assumption should be acceptable 0.4 m above the wind-tunnel floor and over a spanwise extent of about 1.3 m.

Relaminarization

Strong acceleration of a turbulent flow may damp the production terms, to a point that the flow returns to a seemingly laminar state. This is called relaminarization. The acceleration parameter $K = (\nu/U_e^2)(\partial U_e/\partial x)$, proposed by Beasley[9] for two-dimensional

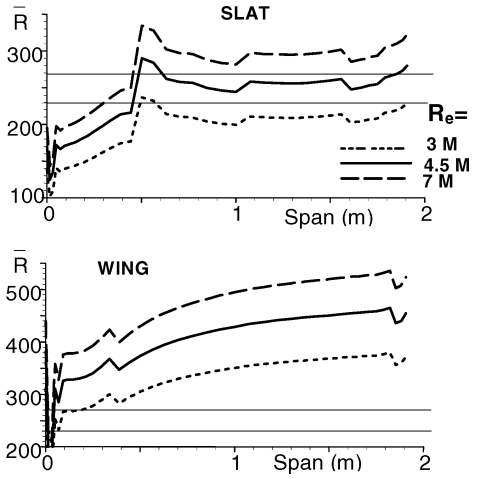

Fig. 7 Spanwise evolution of the contamination Reynolds number ($\varphi = 40$ deg and $\alpha = 10$ deg).

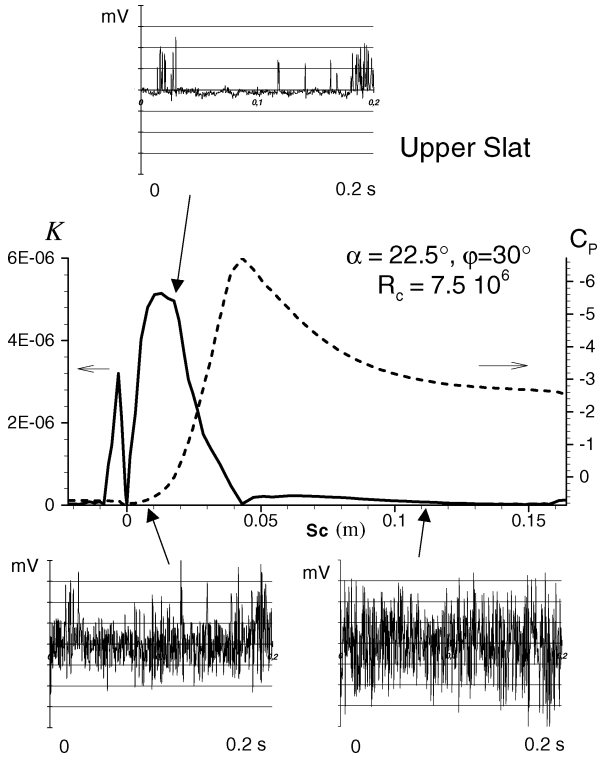

Fig. 8 Observed relaminarization (partial) on the slat upper surface, visible on the hot-film signals.

flow, is a local parameter, independent of boundary-layer parameters, which can be obtained in the preprocessing step together with attachment line transition Reynolds number $\bar{R}$. In three-dimensional flow, K should be evaluated in the streamline direction.[10] Relaminarization of a turbulent boundary layer should be expected if values of K are larger than 5×10^{-6} over a significant distance. Large values have the effect of keeping the boundary layer in a quasi-laminar state, called laminarescent,[10] but as soon as K decreases the turbulence reappears rapidly.

Return to turbulence proceeds as in a bypass transition, without going again through a linear stability stage. A turbulent flow is required upstream of relaminarization, which may be caused by contamination.

Occurrences of partial relaminarization were observed in the experiment, as shown in Fig. 8. Values of K and $-C_p$ (from RANS) are plotted as functions of the curvilinear distance to the attachment line Sc. (Absolute values of K are, in fact, plotted in Fig. 8.) On the attachment line, $K = 0$ by reason of symmetry. Then, the flow accelerates around the leading edge, and K rises to 5×10^{-6}. This maximum is observed at the beginning of the rise of the $-C_p$ curve. Signals from three hot films, located according to the arrows, are also represented. Turbulent signal on the first hot film, near the attachment line, confirms that this case is contaminated. The second hot film shows a sharp reduction of the fluctuation level, caused by the acceleration. Values of K are indeed close to the threshold value of 5×10^{-6}. The last hot film, farther downstream, again shows a turbulent signal.

RANS Computations

The activity, involving ONERA (as main contributor) and Dassault Aviation, was part of a EUROLIFT work package on CFD validation.[11] The main objective of this activity was to provide accurate pressure distribution for boundary-layer calculation inputs.

A structured multiblock mesh of 3.16×10^6 nodes, containing 40 blocks, was generated for the reference configuration $\varphi = 40$ deg and $\alpha_F = 20$ deg), and preliminary calculations showed that a y^+ value below 1 was ensured.

The ONERA computations were carried out using the ONERA elsA software,[12] under the assumption of a fully turbulent flow, at

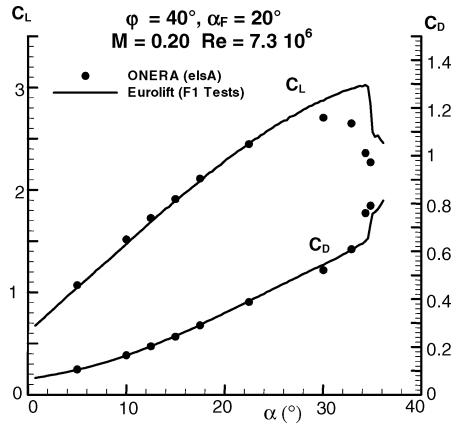

Fig. 9 Computed and measured lift and drag coefficients ($\varphi = 40$ deg and $\alpha_F = 20$ deg).

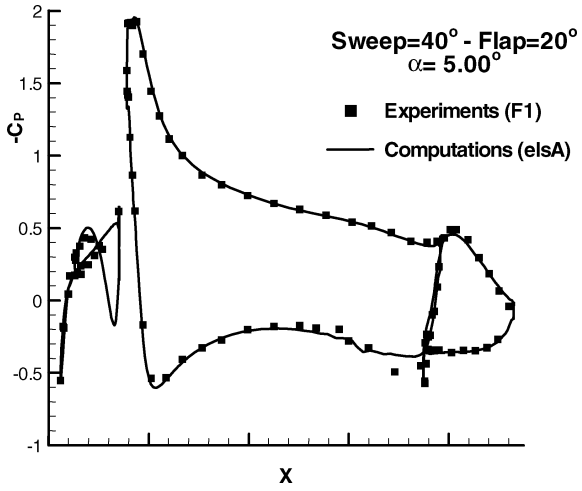

Fig. 10 Pressure distribution at midspan; comparison with experiments for $\alpha = 5$ deg ($M = 0.2$, $Re = 7.5 \times 10^6$, $\varphi = 40$ deg, and $\alpha_F = 20$ deg).

a Reynolds number of 7.5×10^6. The turbulence model used was the Smith's k–l (Refs. 13 and 14). A low-speed preconditioning technique and multigrid algorithms were also used.

Computed global lift and drag coefficients are compared to wind-tunnel measurements in Fig. 9 at a slightly smaller Reynolds number of 7.3×10^6. The agreement between measurements and prediction is good in the linear range, up to about $\alpha = 20$ deg, but maximum lift is underestimated and predicted at a somewhat lower incidence. Differences observed may be due to geometrical details not taken into account in the computations, such as the tracks, model deformation under aerodynamic load, and unsteady flow effects.

The computed pressure distributions are the inputs for the transition prediction study. They allow a better resolution than the measured ones.

Therefore, the quality of their prediction by CFD has to be assessed. Comparisons of computed pressure distributions at midspan with measured ones are presented in Figs. 10 (for $\alpha = 5$ deg) and 11 (for $\alpha = 17.5$ deg) and it can be seen that an excellent correlation is obtained.

Also, a comparison of measured and computed pressure distributions at almost the same poststall lift coefficient (Fig. 12) shows that the stall process is well represented by the computations.

To provide the input data for transition prediction work, a number of selected values of incidence were computed for a single value of sweep, 40 deg, and a single Reynolds number of 7.5×10^6. Based on experimental pressure distributions, it was decided to use the constant sweep law to generate the 30-deg sweep data and to assume independence of the pressure distribution in the range of interest of Reynolds numbers. Thus, transition prediction was executed by the

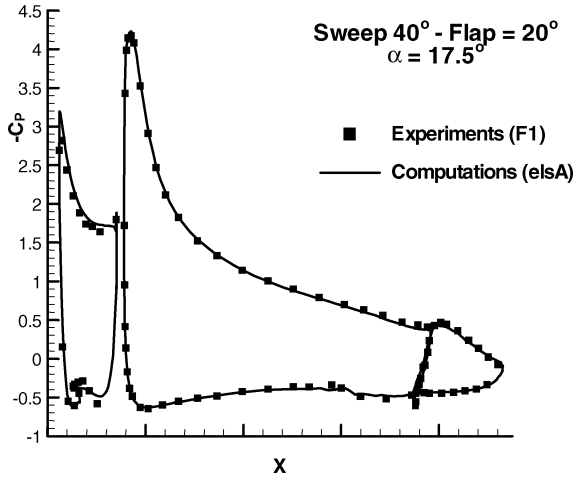

Fig. 11 Pressure distribution at midspan; comparison with experiments for $\alpha = 17.5$ deg ($M = 0.2$, $Re = 7.5 \times 10^6$, $\varphi = 40$ deg, and $\alpha_F = 20$ deg).

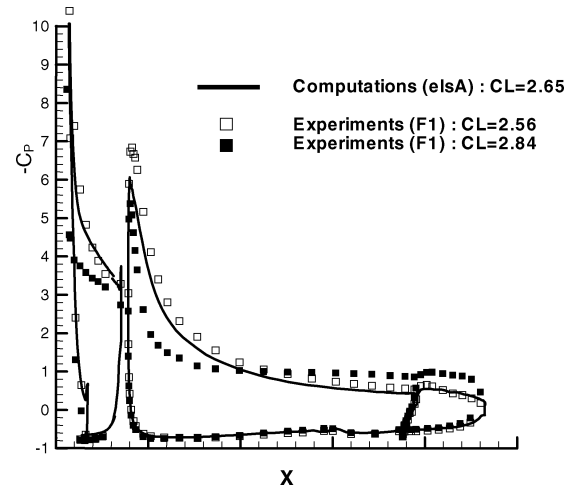

Fig. 12 Comparison CFD to experiments for C_P distributions in poststall conditions. $M_e = 0.2$, $Re = 7.5 \times 10^6$, $\alpha_F = 20$ deg, and $\alpha = 34.8$ and 35.1 deg (experiments)/$\alpha = 33$ deg (CFD).

exclusive use of numerical tools, the results of which were validated at each step by comparison to the experiments.

Transition Prediction

Transition prediction work, involving Airbus Deutschland, CASA and INTA (Spain), CIRA (Italy), and FOI (Sweden), together with ONERA as task leader, was part of a EUROLIFT work package dedicated to CFD improvements.[15] The transition prediction work consisted of a step-by-step validation of tools common to the project partners, implemented into each partner's flow solver, with the aim of predicting contamination, relaminarization, separation, and natural transition. The first two phenomena were correlated to functions of the surface pressure earlier in the paper. The other two, transition controlled by boundary-layer instabilities, and short bubble transition, will now be examined.

Despite the general objective of a RANS-based prediction method for high lift, it was shown at the start of the project that RANS computation of the viscous wall regions could not reasonably provide the precision required for stability calculation and transition prediction. Artificial viscosity allowing rapid convergence and numerical stability is not compatible with precise computation of laminar boundary layers. In two-dimensional flows, transition criteria may be expressed by the use of functions that are insensitive to this. It is not so in three-dimensional flows because characteristics of the velocity profile in the vicinity of its inflection point play a major role on stability. It was, thus, agreed that boundary-layer codes

(infinite swept wing) were necessary tools to guarantee the requested precision. The mean flow pressure distribution was provided by turbulent RANS computations. Once these boundary-layer profiles are obtained, the linear stability theory describes how small, preexisting perturbations may initiate the growth of boundary-layer eigensolutions. Both OS and PSE formulations[16] are commonly used. Under the local (parallel flow) assumption, perturbations are written in a form $A(\boldsymbol{X}, t) = \hat{A}(y)e^{\sigma x}e^{i(\upsilon x + \beta z - \omega t)}$, with $\upsilon, \beta, \sigma, \omega \in R$. Here, (υ, β) are the components of the wave vector, oriented at an angle ψ with respect to the external flow direction. Growth rates σ in OS, or evolution of amplitudes (PSE) can be expressed in term of N factors and correlated to the transition location by the use of the Smith and Gamberoni[17] e^N method.

Stability computations are generally difficult and time-consuming because they require careful initialization and extensive parametric variations. Thus, simplified methods, with potential fully automatic use, are of great interest because they may even be inserted inside the boundary-layer code.

Transition Prediction Based on Simplified Stability Analysis

The simplified stability approach, or database method, provides an estimation of the growth rate σ directly from mean flow parameters and the boundary-layer profile characteristics. The idea is that the Reynolds number variation of growth rates obtained by solution of the exact OS equations can be represented, for a given profile, by the use of two one-half parabolas[4]:

$$\sigma = \sigma_M\left[1 - \left(\frac{R_{\delta_1} - R_M}{R_k - R_M}\right)^2\right] \qquad \begin{aligned} R_k &= R_0 \quad \text{if} \quad R_{\delta_1} < R_M \\ R_k &= R_1 \quad \text{if} \quad R_{\delta_1} > R_M \end{aligned}$$

This parabola model (Fig. 13) requires determination of R_0, R_1, R_M, and σ_M as functions of nondimensionalized frequency $F = 2\pi f\nu/U_e^2$, boundary-layer characteristics, and mean flow conditions. These functions were established from sets of exact stability solutions of Falkner–Skan self-similar profiles in two-dimensional flow. A first model was, thus, created for longitudinal instabilities,[4] based on a two parameters lookup table. These parameters are the incompressible shape factor H_i and the local Mach number M_e.

Crossflow instabilities are inflectional in nature, they are determined by the location and characteristics of the velocity profile inflection point. Given two-dimensional profiles with reverse flow, it was shown that two parameters, $U_i = U(y_i)$ and P_i, may be allowed to represent the growth rate Reynolds dependence.[5]

A purely analytical model was built to this purpose. To represent crossflow instabilities, use of Stuart's theorem (see Ref. 18) and Gaster's relation[19] are necessary. Stuart's theorem states that, in temporal theory, the growth rate σ_ϕ in any direction ϕ can be determined from the stability of the two-dimensional velocity profile projected in the ϕ direction of the original three-dimensional profile. The projected profile is defined as $U_\phi = (\upsilon/k)U + (\beta/k)W, k = \sqrt{(\upsilon^2 + \beta^2)}$, with the reduced frequency $F = 2\pi f\nu/U_\phi^2$. Gaster's relation then provides a relation from temporal to spatial growth rates. This model applies only to traveling crossflow instabilities ($F > 0$), and in a range $|\phi| < 90$ deg.

The two models, for longitudinal and for crossflow instabilities, were later combined. The resulting database method for transition prediction allows, with high efficiency, an estimation of the stability characteristics of three-dimensional boundary layers. Growth rates obtained are integrated to produce envelope N factors exactly, as in the case of exact stability theory.[20] Careful optimization has ensured that, in general, the most amplified frequencies are represented with a precision better than one count in N factor at transition, with transition N factors greater than seven.

One important advantage of the method is that it does not require any initial values, and is, thus, well adapted for insertion into boundary-layer codes. This code was distributed to the project partners for insertions into their own infinite swept wing boundary-layer codes.

It was first decided to validate partners' implementation of the simplified method, given a three-dimensional boundary layer around a 0.3-m chord ONERA D profile in swept-wing configuration ($\varphi = 30$ deg, $M = 25$, $R_c = 1.75 \times 10^6$, and $\alpha = -6$ deg).

Input data were the pressure distributions. Figure 14 shows a comparison of exact local stability results compared to database results for this swept-wing validation case. Maximum difference is about 1 count, with N factors close to 10. Partners' results are illustrated in Fig. 15 for a single frequency of 2 kHz, one of the unstable frequencies. In this exercise, the input data were the pressure distributions, and each one used its own boundary-layer code with the database code. Differences are mostly due to the various boundary-layer codes used.

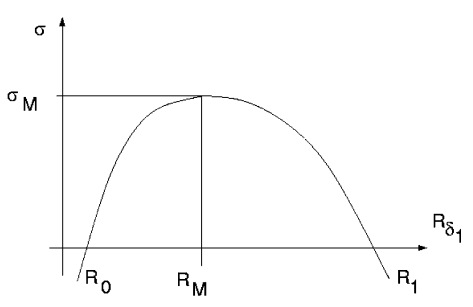

Fig. 13 Growth rate variations represented with parabolas.

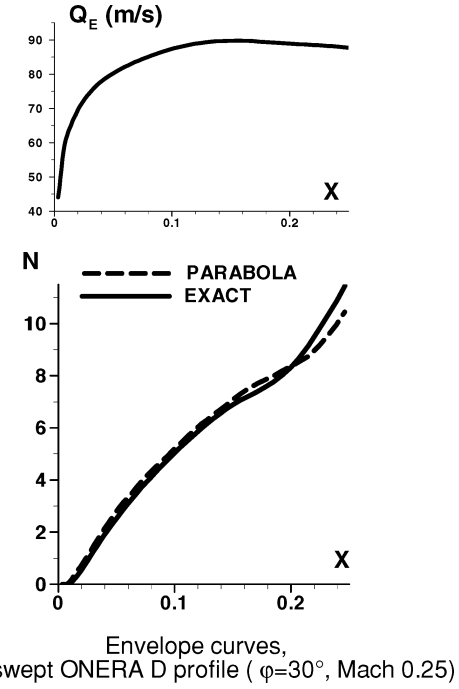

Fig. 14 Database validation on a simple three-dimensional flow ($R_c = 1.75 \times 10^6$ and $\alpha = -6$ deg).

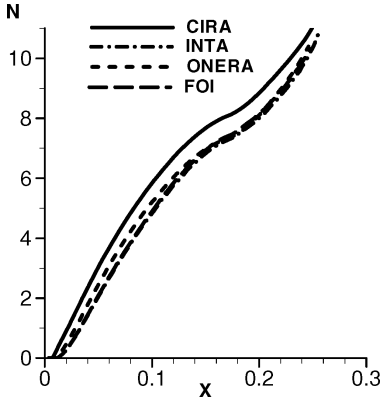

Fig. 15 Partners' results for the ONERA D swept-wing case, $f = 2$ kHz (same conditions as Fig. 14).

Short Bubble Transition

In many high-lift cases, at large incidence, transition to turbulence occurs through laminar separation due to strong positive pressure gradients. Such regions of decelerated flow are always strongly unstable, the instability being related to the inflection point in the velocity profile. Dominant instability is always longitudinal. The large amplifications may cause transition to occur shortly after, if not before, separation. Although the physical aspects are strongly linked, separation is usually detected in the course of the boundary-layer computation; hence, it is found independently of stability calculations.

Another question is related to the length of the separation region and to its physical importance. Most CFD tools will assume instantaneous transition right after detecting separation and will not compute nor estimate the bubble length and its influence on the boundary-layer growth and on the lift coefficient.

Physically, the separated bubble should have a nonzero length. In the experiment, hot films did detect turbulent flow upstream of reattachment line, well visible on the infrared images (Fig. 5b). Rapid boundary-layer growth needs to be accounted for in this region. This problem of transition modeling in a separated flow is not fully solved up to this day.

Application to the AFV Experiment

The three wing elements were analyzed in the course of the project. Attachment line transition and relaminarization were already discussed in the paper and were shown to be predicted at an early stage, based on pressure distribution. Separation and transition caused by the growth of instabilities remain to be examined. Results concerning the flap upper surface will allow a comparison of various exact and simplified stability computations. Then, simplified stability analysis applied to the slat upper surface will be used for transition prediction, and the results will be compared to experimental observations.

Turbulent RANS computation (elsA) provided the pressure distributions over the model. Infinite swept wing theory was then used to generate the velocity distributions, under the assumption of a constant spanwise velocity. Then, task partners used their own boundary-layer codes with the integrated simplified stability method to predict transition. Boundary-layer codes used by the partners were based on conical approximation, infinite swept-wing, and full three-dimensional boundary layer.

In parallel, exact stability calculations were also considered for comparison purposes. In that case, a single set of boundary layers was used because small differences in the boundary-layer codes often cause visible differences in stability results as on Fig. 15. For this work, local and nonlocal (PSE) theories were used. To illustrate these investigations, Fig. 16 shows N factor curves from ONERA, obtained from simplified, local (CASTET[20] code) and nonlocal (FANNIE[21] code) methods for the upper main wing. Nonlocal calculations are performed considering the effects of both nonlocal and curvature terms, and by the use of an envelope of envelopes approach (envelope over constant wavenumber β^* N factors, then envelope over frequencies). Local calculation is done without curvature terms (to be mathematically consistent), by the use of both the envelope strategy and the constant β^* envelope of envelopes. Comparisons are, thus, possible between local and nonlocal results with the envelope of envelopes approach, and between local and database results with the envelope method. For the first comparison, results in Fig. 16 show that the effect of curvature terms is, in this case, larger than that of the nonlocal terms, resulting in lower nonlocal N factors. Curvature terms are known to have a stabilizing effect, whereas nonlocal terms are usually destabilizing. Curvature is large because the attachment line is on the lower side of the flap, and the flow goes around the flap leading edge.

For the second comparison, envelope-method N factors obtained from local and simplified stability calculations are also shown in Fig. 16. Database N factors are slightly larger than exact, local ones in that case. These comparisons show that transition should be predicted at a different N factor by each method. In the project, the same transition N factor of 7.15 was used with the local theory and the simplified approach.

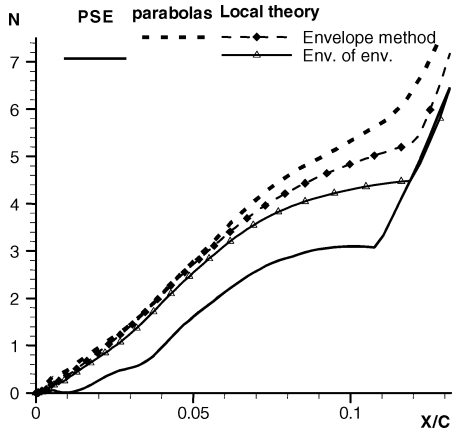

Fig. 16 Exact, local and nonlocal, and simplified stability results for the flap upper surface ($Re = 3.10^6$, $\varphi = 30$ deg, $\alpha = 17.5$ deg, and $\alpha_F = 20$ deg).

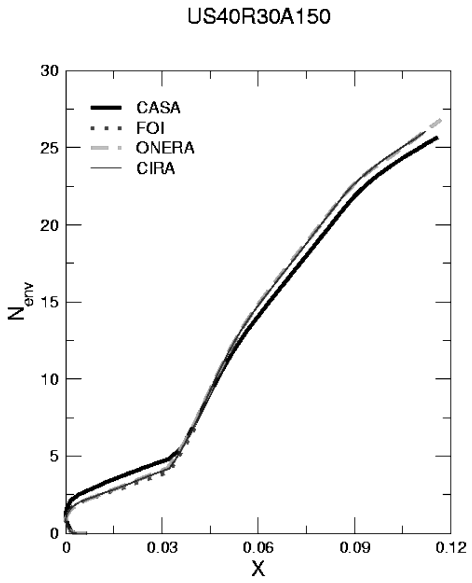

Fig. 17 Database N-factor curves for a typical slat upper surface case; comparison of partners' results ($\varphi = 40$ deg, $R_c = 3 \times 10^6$, $\alpha = 15$ deg, and $\alpha_F = 20$ deg).

Transition prediction was carried out with the database method for the upper slat element. For that case, Fig. 17 shows a typical result, comparing N factor curves from four partners for a case that is again clearly crossflow at the start, then becomes longitudinal past the pressure peak. This is observed at 40-deg sweep, 15-deg incidence, and a chord Reynolds number of 3×10^6. These N factors were obtained starting from the outer flow description and by the use of several boundary-layer codes. Results are similar, transition location would be predicted at 0.045 m ($X_T/C = 9\%$) with an N factor of 7.15. Small differences were analyzed as mostly coming from slightly different estimations on effective sweep angle, which determines the value of the constant spanwise velocity component. In the case of the envelope method, a single N factor is used for both longitudinal and crossflow transitions.

For the same sweep angle and Reynolds number, Figs. 18 and 19 show the predicted transition evolution obtained by FOI and ONERA, compared to the experimental results. The numerical results are represented with lines for transition predictions and symbols for separation predicted in the boundary layer codes.

Transition is of the Tollmien–Schlichting (TS) kind at 5-deg incidence, then at 10 deg, both TS and crossflow instabilities are comparable. Between 10 and 15 deg, transition is of crossflow type, and above 15 deg, separation occurs first.

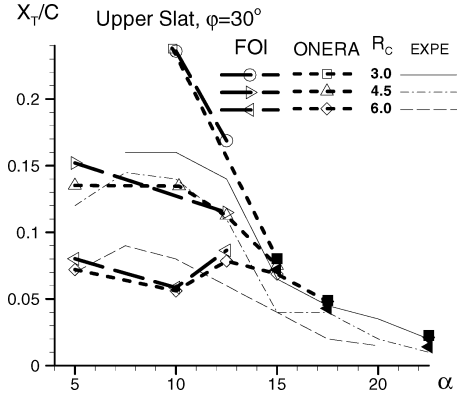

Fig. 18 Slat upper surface experimental and predicted transition evolution with incidence at three values of Reynolds numbers (in millions): $\varphi = 30$ deg, $\alpha_F = 20$ deg, and dark symbols indicate predicted separation.

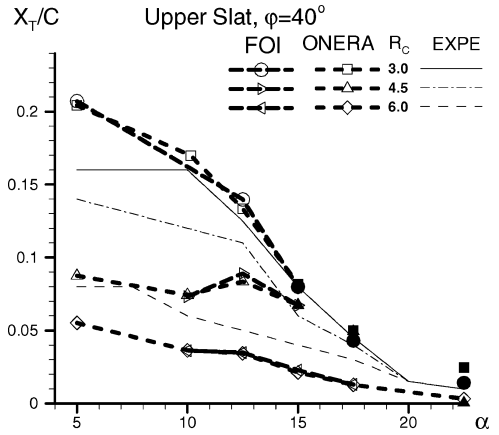

Fig. 19 Slat upper surface transition evolution with incidence at three values of Reynolds numbers (in millions): $\varphi = 30$ deg, $\alpha_F = 20$ deg, and dark symbols indicate predicted separation.

Predictions are seen to match well with the experiments. Discrepancies can be noted at $\varphi = 30$ deg, $Re = 3 \times 10^6$, and $\alpha = 10$ deg with no predicted transition on the element (which ends at $X/C = 0.24$) and also at $\varphi = 40$ deg, $Re = 4.5 \times 10^6$, low incidence, where the difference in transition location reaches 0.05 C_{ref}.

Conclusions

Transition work was very active during the entire EUROLIFT project. Significant progress was achieved, both in understanding the physics governing high-lift transition phenomena and in the validation of prediction tools.

The AFV experiment proved most useful to identify the four most important transition-related phenomena: stability-induced transition, separation, attachment line contamination, and relaminarization. Stability-induced transition has received much attention, and current simplified stability methods allows the expectation of fully integrated predictions in subsonic and transonic infinite swept wing flows, as well as in three-dimensional flows in the coming years.

Predictions of separation and relaminarization starting locations can be considered reliable. Prediction of the extent of laminarescent or separated regions and their quantitative effects on the boundary-layer evolution and on the lift coefficient remains a challenge that will require attention in the next activities. Finally, attachment line contamination can be considered a well-understood and predicted phenomenon that does not require further research work.

Follow-on work is under preparation in the sixth Framework Program of the European Community, the objectives being to correctly treat realistic three-dimensional problems, to improve prediction of the effects of separation and relaminarization, and to integrate fully boundary-layer with RANS approaches.

Acknowledgments

The results presented in this paper have been obtained within the European research project EUROLIFT, under Contract G4RD-CT-1999-00072, which was co-financed by the European Union within the Fifth Research Framework Program. The authors are grateful to the EUROLIFT partners, specially Ardeshir Hanifi, Raffaele Donelli, Jorge Ponsin, Geza Schrauf, Adel Abbas, and Vincente Ibanez for contributing to the results discussed in the paper.

References

[1]Thiede, P., "EUROLIFT—Advanced High Lift Aerodynamics for Transport Aircraft," *Air and Space Europe*, Vol. 3, No. 3/4, 2001, pp. 1–4.

[2]Rudnik, R., Eliasson, P., and Perraud, J., "CFD Methods for Transport Aircraft High Lift Systems," Confederation of European Aerospace Associations, CEAS, Paper 30, London, UK, June 2003.

[3]Séraudie, A., Perraud, J., and Moens, F., "Transition Measurement and Analysis on a Swept Wing in High Lift Configuration," International Council for the Aeronautical Sciences, Aerospace Science and Technology, Vol. 7, No. 8, 2003, pp. 569–576.

[4]Arnal, D., "Transition Prediction in Transonic Flows," *International Union of Theoretical and Applied Mechanics, Transsonicum III Symposium Göttingen*, edited by J. Zierep and H. Oertel, Springer-Verlag, Berlin, 1988, pp. 253–262.

[5]Casalis, G., and Arnal, D., "Database Method–Development and Validation of the Simplified Method for Pure Cross-Flow Instability at Low Speed," ONERA, ELFIN II Tech. Rept. 145, Toulouse, France, Dec. 1996.

[6]Neitzke, K. P., "Using Advanced Measurement Techniques in High Lift Validation Experiments," Confederation of European Aerospace Associations, CEAS, Paper 31, London, UK, June 2003.

[7]Pfenninger, W., "Flow Phenomena at the Leading Edge of Swept Wings," *Recent Developments In Boundary Layer Research*, AGARDograph 97, Pt. IV, Bruxelles, Belgium, May 1965.

[8]Poll, D. I. A., "Some Aspects of the Flow Near a Swept Attachment Line with Particular Reference to Boundary Layer Transition," Cranfield Inst. of Technology, CoA Rept. 7805, Cranfield, England, U.K., Aug. 1978.

[9]Beasley, J. A., "Calculation of the Laminar Boundary Layer and Prediction of Transition on a Sheared Wing," Royal Aeronautical Establishment, Rept. 3787, Farnborough, England, U.K., Oct. 1973.

[10]Arnal, D., and Juillen, J. C., "Leading Edge Contamination and Relaminarization on a Swept Wing at Incidence," *Numerical and Physical Aspects of Aerodynamic Flows IV*, edited by T. Cebeci, Springer-Verlag, 1990, pp. 391–402.

[11]Rudnik, R., "CFD Assessment for 3D High Lift Flows in the European Project EUROLIFT," AIAA Paper 2003-3794, June 2003.

[12]Gazaix, M., Jollès, A., and Lazareff, M., "The elsA Object-Oriented Computational Tool for Industrial Applications," *Proceedings of the 23rd Conference of the International Council for the Aeronautical Sciences (ICAS)*, Toronto, Sept. 2002, Paper 2002-1.10.3.

[13]Smith, B. R., "The k–$k1$ Turbulence Model and Wall Layer Model for Compressible Flows," AIAA Paper 90-1483, June 1990.

[14]Smith, B. R., "A Near Wall Model for the k–l Two Equation Turbulence Model," AIAA Paper 94-2386, June 1994.

[15]Eliasson, P., "CFD Improvements for High Lift Flows in the European Project EUROLIFT," AIAA Paper 2003-3795, June 2003.

[16]Arnal, D., "Boundary Layer Transition: Predictions Based on Linear Theory," *Progress in Transition Modeling*, AGARD Rept. 793, Brussels, 1993, pp. 1–63.

[17]Smith, A. M. O., and Gamberoni, N., "Transition, Pressure Gradient and Stability Theory," Douglas Aircraft Co., Rept. ES 26388, El Segundo, CA, 1956.

[18]Gregory, N., Stuart, J. T., and Walker, W. S., "On the Stability of Three Dimensional Boundary Layer with Application to the Flow due to a Rotating Disc," *Philosophical Transactions of the Royal Society of London, Series A: Mathematical and Physical Sciences*, Vol. 248, No. 943, 1955, pp. 155–199.

[19]Gaster, M., "A Note on the Relation Between Temporally Increasing and Spatially Increasing Disturbances in Hydronamic Stability," *Journal of Fluid Mechanics*, Vol. 14, 1962, pp. 222–224.

[20]Schrauf, G., Perraud, J., Vitiello, D., and Lam, F., "Comparison of Boundary Layer Transition Predictions Using Flight Test Data," *Journal of Aircraft*, Vol. 35, No. 6, 1998, pp. 891–897.

[21]Laburthe, F., "Problème de Stabilité Linéaire et Prévision de la Transition dans des Configurations Tridimensionnelles, Incompressibles et Compressibles," Ph.D. Dissertation, ENSAE, Toulouse, France, Dec. 1992.

[22]Airiau, Ch., "Stabilité Linéaire et Faiblement Non Linéare d'une Couche Limite Laminaire Incompressible par un Système d'Équations Parabolisées (PSE)," Ph.D. Dissertation, ENSAE, Toulouse, France, June 1994.